THE JOURNAL OF PHYSICAL CHEMISTRY A

Article

pubs.acs.org/JPCA

# Dissociation Dynamics and Electronic Structures of Highly Excited Ferrocenium Ions Studied by Femtosecond XUV Absorption Spectroscopy

Adam S. Chatterley,[†,‡] Florian Lackner,[†,‡] C. D. Pemmaraju,[†] Daniel M. Neumark,[†,‡] Stephen R. Leone,[†,‡,§] and Oliver Gessner*[,†]

[†]Chemical Sciences Division, Lawrence Berkeley National Laboratory, Berkeley, California 94720, United States

[‡]Department of Chemistry and [§]Department of Physics, University of California, Berkeley, California 94720, United States

Supporting Information

**ABSTRACT:** The dissociation dynamics of ferrocene are explored following strong field ionization using femtosecond time-resolved extreme ultraviolet (XUV) transient absorption spectroscopy. Employing transitions in the vicinity of the iron 3p ($M_{2,3}$) edge, the dissociation is monitored from the point of view of the iron atom. With low strong field pump intensities ($\approx 2 \times 10^{13}$ W cm$^{-2}$), only ferrocenium cations are produced, and their iron 3p absorption spectrum is reported. It very closely resembles the 3p spectrum of atomic $Fe^+$ ions but is red-shifted by 0.8 eV. With the aid of time-dependent density functional theory calculations, the spectrum is assigned to a combination of doublet and quartet spin states of ferrocenium ions. Ionization with more intense strong field pump pulses ($\geq 6 \times 10^{13}$ W cm$^{-2}$) leads predominantly to the prompt production of ferrocenium ions that dissociate to give the spectral signature of bare $Fe^+$ ions within 240 ± 80 fs. Within the temporal resolution of the experiment (≈40 fs), no spectral intermediates are observed, suggesting that the dissociation process occurs directly from the excited ferrocenium ion and that the bonds between the iron center and both cyclopentadienyl rings are broken almost simultaneously in an asynchronous concerted decay process. No evidence of slower dissociation channels is observed at a pump−probe delay of 250 ps, suggesting that all energy is very rapidly routed into dissociative states.

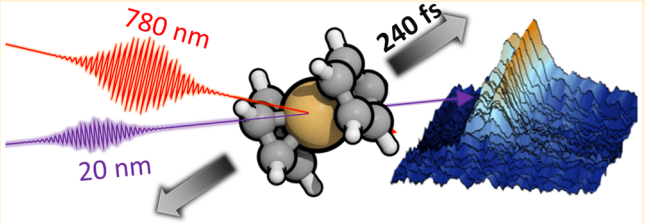


## 1. INTRODUCTION

Ferrocene ($FeCp_2$, Cp = cyclopentadienyl) is a textbook sandwich compound, the study of which has been instrumental in the formulation of organometallic bonding theories.[1,2] Ferrocene is composed of a central iron atom sandwiched between two aromatic cyclopentadienyl rings. Owing to its ease of oxidation, it is commonly used as an electrochemical reference species, and it has recently shown promise as an electrolyte for dye-sensitized solar cells.[3] Exploring the electronic structure and dynamics of both $FeCp_2$ and its cation $FeCp_2^+$ is important from a fundamental point of view for these applications, and more generally for understanding the ground and excited state dynamics in organometallic systems. In this study, we employ femtosecond time-resolved extreme ultraviolet (XUV) absorption spectroscopy[4,5] to glean insight into the electronic structure and dynamics of both ferrocene and ferrocenium after strong field ionization with an intense near-infrared (NIR) laser pulse.[6,7]

Valence UV−vis absorption spectroscopy,[8−11] coupled with ab initio calculations[12−15] and hard X-ray emission spectroscopy,[16] has provided insight into the electronic structure of ferrocene. The frontier orbitals are nonbonding metal d orbitals, and the highest occupied bonding orbitals are formed from interactions of the remaining d orbitals with the $\pi$ system of the aromatic rings. With XUV photons ($h\nu \approx 60$ eV, iron $M_{2,3}$ edge), absorption from the iron 3p inner shell is observed.[17,18] The absorption spectrum in this region consists of broad structures spanning photon energies of ∼55−70 eV, which have been loosely assigned to excitation from the Fe 3p orbitals to the lowest unoccupied molecular orbital (LUMO), an antibonding orbital primarily of d character. The XUV absorption spectrum also sits atop a large (∼50%) background from valence ionization. Despite the rather broad, mostly featureless character of the $FeCp_2$ ground state XUV absorption spectrum, the high degree of localization of Fe 3p electrons and the corresponding core-to-valence transitions may be used to track strong-field initiated dynamics in the molecule exclusively from the perspective of the iron atom. The significant dependence of inner shell transitions on the local valence electronic structure around a well-defined reporter atom results in new opportunities to monitor both electronic and structural dynamics in strong-field ionized ferrocene that are at the center of this work.

**Received:** September 26, 2016
**Revised:** November 3, 2016
**Published:** November 9, 2016





DOI: 10.1021/acs.jpca.6b09724
J. Phys. Chem. A 2016, 120, 9509−9518

Recently, Yatsuhashi and co-workers have demonstrated that strong field ionization of gaseous $FeCp_2$ with a femtosecond NIR pulse yields multiply charged $Fe^{n+}$ ions.[19] Using time-of-flight mass spectrometry, the authors found that, as the NIR intensity is increased beyond $1 \times 10^{15}$ W cm$^{-2}$, Fe ions with charge states as high as $Fe^{6+}$ are observed. Intriguingly, dissociation leading to the loss of a single cyclopentadienyl ring was a minor channel compared to double ring loss. This observation was interpreted in terms of a stepwise reaction mechanism, whereby $FeCp_2^+$ initially dissociates to give $FeCp^+$ and Cp• products, and the ionic species further dissociates to give bare $Fe^+$ and a second Cp• radical. This mechanism was further justified by a relative absence of charged organic species in the mass spectrum.

In the present study, we use femtosecond time-resolved transient XUV absorption spectroscopy to study the product dynamics of ferrocene following SFI with NIR pulses in the intensity regime of $\sim 2 \times 10^{13}$ to $1.4 \times 10^{14}$ W cm$^{-2}$. The results complement previous mass spectrometry experiments that, while elegantly demonstrating the efficient production of highly charged iron ions from a ferrocene precursor, provide limited insight into the detailed dissociation mechanisms.[19] We first explore the XUV spectra of ferrocenium cations, which we assign with the aid of time-dependent density functional theory calculations. The observed iron 3p absorption spectrum of ferrocenium is composed of both $^2FeCp_2^+$ and $^4FeCp_2^+$ spin states. It is reminiscent of the bare $Fe^+$ 3p absorption spectrum, which can be justified by the fact that the valence hole may have a predominant iron d orbital character. Moreover, we measure the time dependence of the XUV spectrum at a NIR intensity of $\sim 6 \times 10^{13}$ W cm$^{-2}$. We find that, within the temporal resolution of the experiment (40 fs), dissociation to give isolated $Fe^+$ proceeds directly on a 240 fs time scale, and it does not follow a stepwise mechanism as might be anticipated.

## 2. METHODS

The XUV transient absorption experiment has been described in detail elsewhere,[5,20] so only a brief description is given here, with an emphasis on the modifications that permit gas phase studies on molecules from volatile solid compounds. Ferrocene (SigmaAldrich, 99%) is loaded into a heated copper oven with a ceramic sample cell fixed to it and inserted into the vacuum chamber. The sample cell is a vertically aligned cylinder with a 1 mm internal diameter and has 750 $\mu$m holes drilled through both sides to allow light to be transmitted perpendicular to the cylinder axis. To introduce a significant vapor pressure (~2.3 Torr) of ferrocene, the solid compound is heated to ~100 °C. A copper jacket heated to ~150 °C is placed over the sample cell to prevent recrystallization. A liquid nitrogen cooled cryotrap is used to capture spent ferrocene and prevent damage to the vacuum pumps. Soot and debris from ionized ferrocene build up on the entrance holes of the sample cell when using a strong NIR pump pulse, necessitating periodic (approximately every half hour) venting and cleaning of the sample cell.

To perform XUV transient absorption spectroscopy, the output from a femtosecond Ti:sapphire laser system (3 kHz, 780 nm central wavelength, 3.3 mJ pulse$^{-1}$) is split into two beams using a 50:50 beamsplitter. The first beam provides the NIR strong field pump pulse. This beam is sent through a motorized, computer controlled delay line and is then focused into the sample cell with an $f/30$ lens. A half-wave plate and a thin film polarizer allow continuous variation of the pump beam intensity, without changing its spatiotemporal characteristics. The focused intensity of the light was varied from approximately $2 \times 10^{13}$ W cm$^{-2}$ to $1.4 \times 10^{14}$ W cm$^{-2}$ as determined using a power meter to measure the pulse energy, and a CCD beam profiler is used to measure the focal spot size ($85 \pm 15$ $\mu$m). The pulse duration for the NIR pulse was 37 fs, determined using frequency-resolved optical gating (FROG). The intensity calibration has been confirmed by measuring the ratio of $Xe^{2+}$ to $Xe^+$ ions produced by the strong field.[21] We note, however, that the exact determination of the NIR field strength in the interaction volume is challenging, and we conservatively estimate an error of within a factor of 2 on absolute intensity measurements. Errors in relative intensities between separate measurements are dominated primarily by the precision of the pump−probe spatial overlap, and we estimate an error of 10% for these comparisons. The second beam is used to produce XUV pulses with photon energies ranging from 48 to 70 eV, by the process of high harmonic generation (HHG).[22] The NIR beam is focused with an $f/40$ lens onto the exit foil of a semi-infinite gas cell, filled with neon gas at a pressure of 80 Torr. A 300 nm thick Al foil placed at a distance of 0.8 m behind the HHG cell exit rejects the remaining NIR light, while transmitting most of the XUV light. A toroidal mirror focuses the XUV light into the sample cell, crossing the pump beam at a 1° angle. After the sample cell, a variable line space grating is used to disperse the XUV light onto an X-ray CCD camera to record the transmitted spectrum. The pump−probe overlap is optimized by maximizing the 4d absorption signal from $Xe^+$ ions produced by SFI.[5] The appearance of this signal provides time zero for the pump−probe delay and an instrument response function of 40 fs full-width-at-half-maximum (fwhm). Note that the IRF is very similar to the NIR pulse duration, as the XUV pulse has a significantly shorter duration. To protect both the toroidal mirror and the CCD camera from ferrocene vapor, two additional 200 nm thick Al foils are used to isolate both sides of the interaction chamber from the rest of the vacuum system. Energy calibration is performed using the characteristic 4d absorption lines of both Xe atoms (65.11, 66.38, and 67.04 eV) and $Xe^+$ ions (55.39 and 56.08 eV), which are also used to derive the spectral resolution of ~100 meV (fwhm).[5]

All transient absorption spectra are referenced to the XUV spectrum recorded with the pump laser blocked. To minimize the impact of temporal variations in the high harmonic spectrum on the transient absorption spectra, an optical chopper is used to block the pump beam at a rate of 4 Hz, corresponding to every other spectrum recorded by the CCD camera. This allows the reference to be recorded (nearly) simultaneously with the signal. Transient absorption spectra are reported in ΔOD (change in optical density), defined for a given photon energy $E$ and pump−probe delay $t$ as $\Delta OD(E,t) = \log_{10}(I_{ref}(E)/I_{sig}(E,t))$. The signal and reference intensities $I_{sig}$ and $I_{ref}$ refer to the amount of transmitted XUV light when the pump beam is on and off, respectively. The spectrum for each delay is an average of ~100 scans, with 5 s of exposure per scan. The statistical scatter of the ~100 independent scan results is used to derive the reported error bars, which represent the uncertainties of the mean values within 95% confidence intervals.

First-principles time-dependent density functional theory (TDDFT)[23] calculations are performed in order to support the interpretation of the recorded XUV absorption spectra. The neutral and singly ionized configurations of $FeCp_2$ as well as singly ionized $Fe^+$ ions are considered in this analysis. Density


DOI: 10.1021/acs.jpca.6b09724
J. Phys. Chem. A 2016, 120, 9509−9518

functional theory[24,25] based structural optimizations of the molecular species $FeCp_2$, singly ionized doublet $^2FeCp_2^+$, singly ionized quartet $^4FeCp_2^+$, and singly ionized quintet $^5FeCp^+$ with geometries initialized in the eclipsed (D5h) configuration, are carried out with the ORCA program[26] employing the B3LYP[27,28] functional together with the def2-TZVP(-f) basis set.[29] The resolution of identity (RI) approach,[30,31] with the def2-TZV/J auxiliary basis set,[32] is utilized to speed-up two-electron integral transformations.

Fe $M_{2,3}$-edge XUV absorption spectra of molecular $FeCp_2$, $^2FeCp_2^+$ in ground and first excited states, $^4FeCp_2^+$, $^5FeCp^+$, and $Fe^+$ ions in the $4s^13d^6$ and $4s^03d^7$ configurations are then calculated using the restricted-energy window (REW)[33] variant of linear-response TDDFT[34] as implemented in the Q-Chem[35] code. The TDDFT calculations are carried out within the Tamm-Dancoff approximation[36] (TDA) at the B3LYP/def2-TZVP level.[29] At least 100 excited state roots are calculated for each configuration, producing spectra that extend roughly over a 10 eV range in the region of interest. Relativistic corrections are not explicitly included in the TDDFT-TDA calculations, but an Fe 3p spin−orbit splitting of 0.7 eV[37] is incorporated into the calculated spectra as a postprocessing step.

Additionally, Fe $M_{2,3}$-edge spectra for all of the species mentioned above are calculated using the restricted open-shell configuration interaction singlets DFT/ROCIS[38] scheme as implemented in the ORCA program.[26] The B3LYP functional is employed in this context, in conjunction with the def2-TZVP(-f) basis set and RI approximation utilizing the def2-TZV/J auxiliary basis set. The three parameters c1, c2, and c3 within the DFT/ROCIS scheme are set to the same values c1 = 0.18, c2 = 0.20, and c3 = 0.40 employed by Roemelt et al. for the B3LYP functional.[38]

The restricted energy window (REW) TDDFT approach[33] is of broad utility for calculating inner-shell excitation spectra of molecules. However, given the open-shell $3p^53d^{N+1}$ electronic final states accessed in Fe $M_{2,3}$-edge excitations, a rich multiplet structure is expected in the XUV spectra of all of the Fe based species involved in this study, and a single-determinant approach such as TDDFT is not expected to be quantitative.[38] Multideterminantal theories are in principle necessary for an accurate description of such systems, but higher-order wave function methods are generally impractical for inner-shell spectra of medium-sized molecules. Recently, Roemelt et al. proposed a computationally efficient DFT/ROCIS[38] scheme for the calculation of transition metal L-edge X-ray absorption spectra accounting for some of the multiplet character in 2p → 3d X-ray transitions.[38] Therefore, in addition to REW-TDDFT-TDA, we also utilize the DFT/ROCIS scheme to calculate Fe $M_{2,3}$-edge absorption spectra for various species of interest. We find, however (see SI), that REW-TDDFT-TDA and DFT/ROCIS yield qualitatively similar results in the present context with some differences in overall line shapes. Furthermore, given the relatively broad and weakly structured spectra measured in the experiment, it is not possible to definitively ascertain the accuracy of either theory in relation to the current set of experiments. We expect nevertheless that the calculated spectra should be qualitatively correct and thus useful for interpreting general trends in the experimental spectra. In the analysis that follows we utilize the REW-TDDFT-TDA results and note that no rigid shift was applied to the calculated excitation energies.

## 3. RESULTS

Figure 1 shows transient XUV difference absorption spectra of $FeCp_2$, recorded 1 ps after strong field ionization with varying

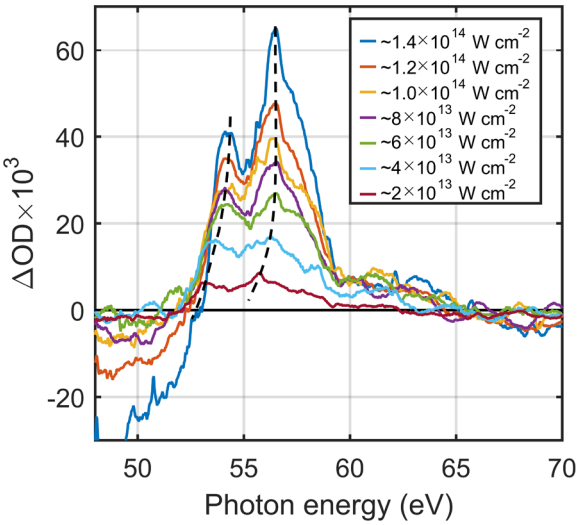


**Figure 1.** Transient Fe 3p edge absorption spectra of ferrocene 1 ps after ionization with a near IR strong field pulse of varying intensity. Positive features correspond to enhanced absorption, while negative ones indicate a decrease compared to the neutral parent molecule. Black dashed lines illustrate a systematic shift of the peak maxima, which is due to an increase in $Fe^+$ signals compared to $FeCp_2^+$ signals; see text for details.

intensities of the 780 nm pump pulse. Considering first the lowest intensity spectrum, ~2 × $10^{13}$ W $cm^{-2}$ (dark red curves in Figures 1 and 3d), a broad double peak feature is visible around 55 eV, with a tail extending out to ~62 eV. Two maxima are observed at 53.0 and 55.7 eV. As the laser intensity is increased, several changes can be observed in the 1 ps spectrum. The signal increases in intensity, the two peaks broaden slightly, and their maxima shift from 53.0 and 55.7 eV to 54.1 and 56.5 eV, respectively. This trend is illustrated by the dashed lines in Figure 1, which trace the peak maxima. Additionally, as the laser intensity is increased, a spectral bleach becomes prominent at photon energies <52 eV. An additional presentation of the data in Figure 1, with confidence intervals, is available in the SI.

In addition to the spectra at long time delays, we have also explored the time dependence of the XUV difference absorption spectrum at an intermediate NIR pump intensity of a ~6 × $10^{13}$ W $cm^{-2}$. Figure 2 presents a waterfall representation of the difference spectrum as a function of time, following the NIR pump pulse. When the strong field pump and XUV probe pulses overlap at $t$ = 0, a broad absorption feature is promptly observed, ranging from ~53 to 65 eV. In the pre-edge valence absorption region ($h\nu_{probe}$ < 53 eV), a corresponding prompt depletion appears. Growing in on a slower (hundreds of femtoseconds) time scale, two peaks can be seen, with energies corresponding to those assigned to $Fe^+$ in the 1 ps spectrum (54.1 and 56.5 eV).[39] Additionally, in the pre-edge region, a slight recovery is observable, on a time scale similar to the appearance of the sharp peaks.



DOI: 10.1021/acs.jpca.6b09724
J. Phys. Chem. A 2016, 120, 9509−9518

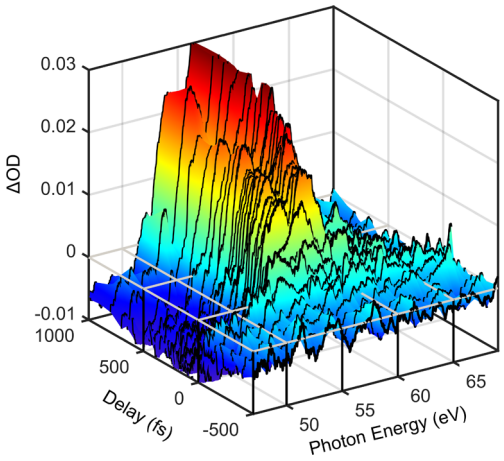


**Figure 2.** Waterfall representation of the XUV difference absorption spectrum of $FeCp_2$, following strong field ionization with a ~$6 \times 10^{13}$ W $cm^{-2}$ NIR laser pulse. Shortly after $t = 0$, a sharp double-peaked structure grows in at around 53−65 eV, along with spectral depletion at photon energies <52 eV.

## 4. ANALYSIS

**4.1. Long-Time Pump−Probe Spectra.** To interpret the spectra, we use a combination of first-principles calculations, together with comparison with the existing literature. To benchmark the calculations, the static spectrum of neutral $FeCp_2$ is first calculated (shaded area in Figure 3a) and compared with the literature spectrum (green curve in Figure 3a).[18] The REW-TDDFT approach does not take into account the large background of high energy valence excitations that overlap with the Fe $M_{2,3}$-edge and fails to describe the broad features in the spectrum, although the energies of the features around 60 eV at the rising $M_{2,3}$-edge are reproduced within an error of ~1 eV. A second benchmark, of isolated $Fe^+$ cations, is displayed in Figure 3b as shaded areas. To reproduce the main features of the literature spectrum (black line in Figure 3b),[39] two configurations are required: the $4s^13d^6$ ($^6D$) ground state configuration along with the metastable $4s^03d^7$ ($^4F$) configuration, which is also expected to be present.[39] The feature at 56.1 eV is assigned to 3p → 3d transitions from a $4s^13d^6$ initial state, while the feature calculated at 54 eV is due to a combination of 3p → 4s transitions in the $4s^13d^6$ state and 3p → 3d transitions in the $4s^03d^7$ configuration. The present theory cannot predict the relative fractions of $4s^13d^6$ and $4s^03d^7$ configurations produced in the SFI process, but the former is expected to be preponderant.[39] With the above peak assignments, TDDFT qualitatively matches the shapes and the energies of the experimental spectra.

Interpretation of the lowest intensity difference spectrum (reproduced as the red line in Figure 3d) can be aided by comparison with the ion yield data by Yatsuhashi et al., which show that at these intensities the $FeCp_2^+$ parent ion is the only major ionic product.[19] The broad features can then be assigned to excitation of Fe 3p electrons into vacancies in the nonbonding frontier orbitals of the parent molecular ion. The assignment of the low-intensity NIR pump differential spectrum to $FeCp_2^+$ is confirmed by the calculations. The shaded areas in Figure 3d show the computed spectra for both the $^2FeCp_2^+$ ground state (blue filled) and the $^4FeCp_2^+$ quartet state (green filled). Both taken together, there is reasonable agreement with the experimental 1 ps spectrum around 52−57 eV, and neither spectrum alone can reproduce the doublet

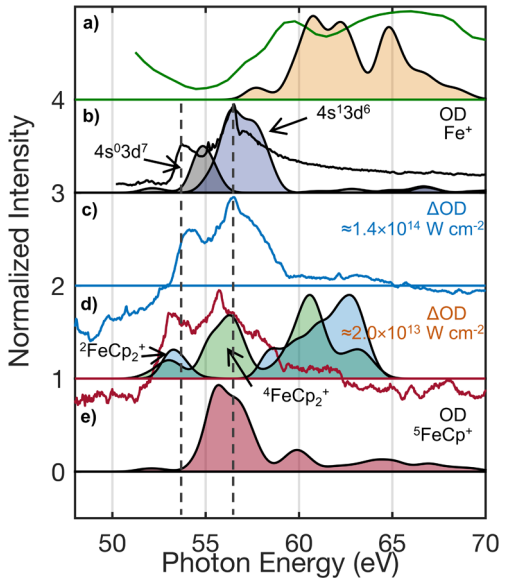


**Figure 3.** (a) Normalized static XUV absorption spectrum of $FeCp_2$ (green, taken from ref 18), in comparison with the B3LYP ab initio calculated absorption (orange filled curve, see text for details). (b) The static $Fe^+$ reference spectrum (black curve, taken from ref 39), in comparison with the calculated spectra for the two lowest energy $Fe^+$ configurations (gray and blue filled curves). (c) The ΔOD transient spectrum recorded 1 ps after ionization with the highest NIR pump intensity ($1.4 \times 10^{14}$ W $cm^{-2}$, blue curve). (d) The ΔOD transient spectrum recorded 1 ps after ionization with the lowest NIR pump intensity ($2.0 \times 10^{13}$ W $cm^{-2}$, red curve), in comparison with the calculated static spectra for both the doublet (blue filled) and the quartet (green filled) configurations of $FeCp_2^+$. (e) The calculated spectrum (red filled) of ferrocene cations following the loss of a single Cp ring, $^5FeCp^+$. Note that the calculated spectra are static absorption not ΔOD, which accounts for the discrepancy around 60−65 eV that is affected by overlapping signals from parent depletion and product emergence (see text). As a guide to the eye, black dashed lines illustrate the peak positions of the experimental $Fe^+$ spectrum. All calculated spectra are scaled arbitrarily for ease of comparison.

structure observed. Although both the doublet and quartet states are required to reproduce the experimental spectrum, we cannot rule out contributions from other configurations such as a low-energy HOMO → LUMO excited state $^2FeCp_2^+$*. The spectrum for this species is shown in Figure S3 in the SI and is broadly compatible with the experimental spectrum, although carries weak oscillator strength in the 52−57 eV spectral region. The peak at 53.0 eV is assigned to Fe 3p core state excitations to an empty nonbonding $e_{2g}$ like final state orbital in $^2FeCp_2^+$, superimposed upon excitations in the $^4FeCp_2^+$ configuration (Figure 4a), while the 55.7 eV peak results from excitations to a weakly antibonding $e_{1g}$ like orbital in the $^4FeCp_2^+$ configuration (Figure 4b). It appears therefore that the spectrum we have assigned to $FeCp_2^+$ is a combination of both spin states. Unlike the Koopman's picture, which predicts the 53.0 eV peak to belong to an excited species, instead we find that the dominant peak at 55.7 eV is the signature of the quartet and the peak at 53.0 eV is a combination of both the doublet and quartet spin states. This counterintuitive result highlights the need for relatively high level calculations when assigning transient XUV spectra of species such as ferrocene.

Note that, while the calculated $FeCp_2^+$ spectra have significant intensity around 60−65 eV, the experimental difference absorption does not. This reflects a difference in


DOI: 10.1021/acs.jpca.6b09724
J. Phys. Chem. A 2016, 120, 9509−9518

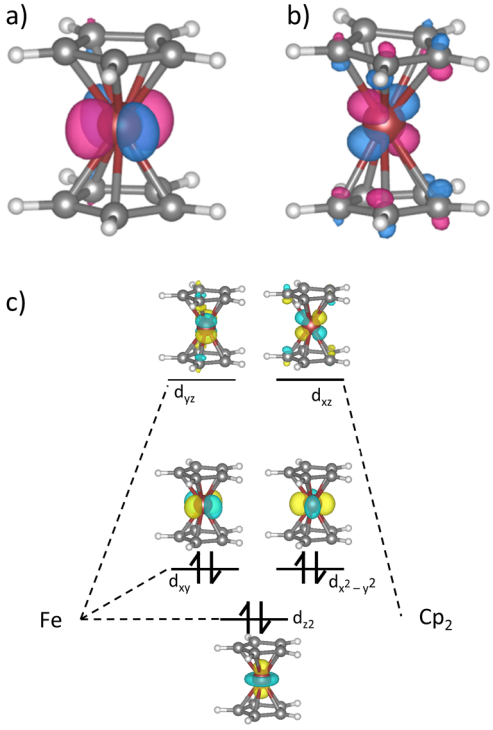


**Figure 4.** (a) Valence molecular orbital of $e_{2g}$ like symmetry that is involved in the 3p → valence transitions primarily responsible for the 53 eV peak in Figure 3d. (b) Valence molecular orbital of $e_{1g}$ like symmetry that is involved in the 3p → valence transitions predominant in the 55.7 eV peak in Figure 3d. The orbital isosurfaces are plotted at 10% of their maximum value. (c) Molecular orbital diagram and plotted isosurfaces of the frontier orbitals of $FeCp_2$. Note that the spacing between energy levels is illustrative, not quantitative.

the quantities being displayed here: the calculated spectra are absolute absorption spectra, while the experimental spectra are differential absorption measurements, relative to the spectrum of neutral $FeCp_2$ without the pump laser. The lack of intensities in 60−65 eV range of the experimental difference spectra is most likely caused by overlapping signals from parent molecule depletion and ionic species emergence, as will be discussed further down.

The highest intensity trace from Figure 1 has been reproduced as the blue trace in Figure 3c. Based on ion yield data,[19] only $FeCp_2^{2+}$ or atomic $Fe^+$ ions are anticipated to be major channels at power densities beyond $10^{14}$ W cm$^{-2}$ (in addition to $FeCp_2^+$). A comparison with the literature spectrum of $Fe^+$ (black curve, Figure 3b)[39] strongly suggests that the predominant spectral contributions beyond those from $FeCp_2^+$ stem from XUV absorption of bare $Fe^+$ ions. Additional molecular features, however, such as doubly charged $FeCp_2^{2+}$ ions, may also contribute to the spectrum. Within our signal-to-noise, no neutral or doubly or higher charged Fe ions are visible, even at the highest laser intensity. All $Fe^{n+}$ ions ($n \leq 3$) possess characteristic sharp spectral lines in the wavelength range of this study.[40] This observation confirms that our maximum laser intensity is less than $2 \times 10^{14}$ W cm$^{-2}$, since at this intensity equal amounts of $Fe^+$ and $Fe^{2+}$ should be produced.[19] Note that the trends illustrated in Figure 1 cannot be the result of a (dynamic) Stark effect since the pump−probe delay of 1 ps is more than 1 order of magnitude beyond the temporal overlap region of the NIR-pump and XUV-probe pulses as characterized by the 40 fs (fwhm) apparatus function.

A second possibility that must be considered is a contribution of ferrocene cations following single ring loss, $FeCp^+$. In ion yield experiments very little of this species was observed compared to the double ring loss $Fe^+$ product;[19] however, it is feasible that single ring loss occurs in less than 1 ps, and the second ring is lost on a much slower time scale. To test for this possibility, the Fe $M_{2,3}$-edge absorption spectrum of the ground state of a single ring $^5FeCp^+$ ion calculated at the TDDFT-TDA level is shown in Figure 3e. The most notable feature in the spectrum of the $^5FeCp^+$ ion (red filled) is a double peak structure around 55.5−56.5 eV that resembles the line shape of the $Fe^+$ $4s^13d^6$ atomic ion but is red-shifted so that it coincides energetically with the 56 eV peak of the $^4FeCp_2^+$ configuration. The line shape does not resemble the sharp peaks found in the $Fe^+$ ion. This $^5FeCp^+$ 55.5−56.5 eV feature mainly involves Fe 3p core transitions into valence states with predominant Fe 3d and Fe 4s character localized around the Fe site (see Figure S4 in the SI). Unlike the $^4FeCp_2^+$ configuration, however, the $^5FeCp^+$ ion exhibits a significant loss of spectral weight in the 58−61 eV range relative to the neutral parent molecule. Thus, while some contribution of $^5FeCp^+$ to the 55.7 eV ΔOD feature in the experiment cannot be ruled out, a dominant role for this configuration would be inconsistent with the lack of a strong depletion ΔOD signal in the 58−61 eV range.

An additional prominent feature that becomes stronger as the pump laser intensity increases is a bleach of absorption at energies <52 eV. These energies are well below the iron $M_{2,3}$-edge, so this feature cannot be attributed to Fe 3p inner shell excitation. Instead, it must correspond to excitation of valence electrons to the ionization continuum. This interpretation is consistent with the fact that in the static XUV absorption spectrum of ferrocene, the LUMO ← $Fe_{3p}$ peak was observed on top of a very large background, which was also attributed to valence absorption.[17,18] Following strong field ionization, the bleach in this region must correspond to a loss of the corresponding valence states, that is, fragmentation and/or ionization of the parent molecule. The behavior of this bleach feature thus provides a probe of the molecule from the point of view of the valence states, in addition to the atom specific iron probe at higher photon energies. The complementarity of the two types of signals will be used below as a consistency test to gain a more complete picture of the molecular ion dissociation dynamics.

### 4.2. Temporal Evolution of XUV Absorption Spectra.

To elucidate the temporal evolution of strong field ionized ferrocene in greater detail, transient XUV absorption spectra were recorded for multiple pump−probe delays at a pump pulse intensity of ~$6 \times 10^{13}$ W cm$^{-2}$ (Figure 2 and 5). All plots in Figure 5 show differences in optical density ΔOD with respect to the $FeCp_2$ ground state absorption spectrum. Figure 5a shows a false-color map of the measured pump−probe delay dependent differential XUV absorption spectrum with time progressing along the horizontal and energy along the vertical axis.

The dynamics of the features at 56.5 eV and <52 eV can be seen more clearly in Figure 5c, which shows the mean intensities within the energy intervals 56−57 eV (blue) and 47−52 eV (red) as a function of pump−probe delay. Two time scales are clearly evident in the rise of the blue signal, while a prompt decrease followed by a slower recovery can be seen in the red signal. In order to analyze the dynamic trends more quantitatively, the time-resolved spectra shown in Figure 5a are


DOI: 10.1021/acs.jpca.6b09724
J. Phys. Chem. A 2016, 120, 9509−9518

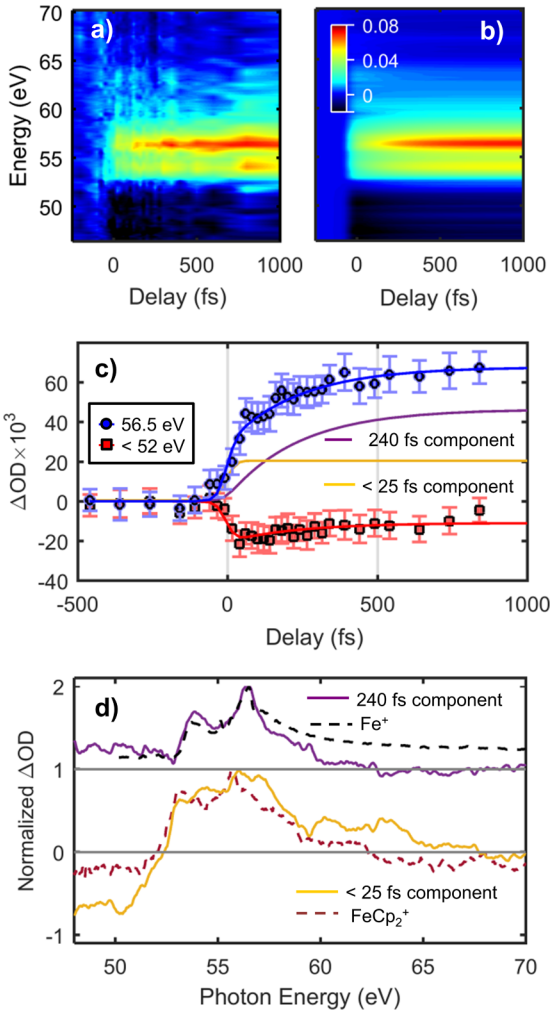


**Figure 5.** Temporal evolution of the XUV absorption spectrum of $FeCp_2$ after excitation with a ~$6 \times 10^{13}$ W cm$^{-2}$ NIR laser pulse. All plots show differences in optical density ΔOD with respect to the $FeCp_2$ ground state absorption spectrum. (a) Measured absorption dynamics as a function of pump−probe delay (horizontal) and XUV absorption energy (vertical). (b) Global fit to the data in panel a using two components with single exponential rise functions and arbitrary spectra. (c) Transient ΔOD around 56.5 eV (blue circles), corresponding to the dominant $Fe^+$ peak, and <52 eV (red squares), corresponding to valence-to-continuum absorption. Error bars are 95% confidence intervals. The results of the global fit in panel b are shown as solid lines through the data points. The temporal evolution of the two independent fit components that contribute to the blue $Fe^+$ curve are represented by the purple and yellow curves. (d) Normalized spectra associated with the two independent fit components (yellow and purple solid curves). Plotted alongside for comparison as dashed curves are the normalized spectra of $FeCp_2^+$ (dark red, from the 1 ps spectra with $2 \times 10^{13}$ W cm$^{-2}$ pump intensity) and $Fe^+$ (black, from ref 39). The upper panel of d presents the 240 fs component, compared to the $Fe^+$ spectrum, while the lower panel presents the rapidly rising component, compared to the $FeCp_2^+$ spectrum.

described by a global fit, using the standard trust-region least-squares algorithm implemented in MATLAB. The fit function is based on two independent components and may be described by

$$\mathrm{TRXAS} = \mathbf{A}_1(E) \times \mathbf{f}_1(t) + \mathbf{A}_2(E) \times \mathbf{f}_2(t) \quad (1)$$

where $\mathbf{A}_n(E)$ is a column vector containing the (unknown) spectral intensity of the $n$th component as a function of probe photon energy, which is derived by the fit procedure, and $\mathbf{f}_n(t)$ is a row vector containing the temporal evolution of the $n$th component:

$$\mathbf{f_n}(t) = \left[1 - \exp\left(-\frac{t - t_0}{\tau_n}\right)\right] * g(t) \quad (2)$$

Here, $\tau_n$ is the characteristic rise time of the $n^{th}$ component, and $*g(t)$ indicates a convolution of the ideal time trace with the Gaussian instrument response function. Only the two time constants $\tau_n$, and the spectral amplitudes $\mathbf{A}_n(E)$ ($n$ = 1, 2) are free fit parameters, while the instrument response $g(t)$ and time zero $t_0$ of the pump−probe delay axis are measured independently using atomic Xe as described in the experimental section. Note that a signal depletion is described by negative values of the spectral intensities $\mathbf{A}_n(E)$.

A false color plot of the resultant fit is shown in Figure 5b, illustrating good qualitative accord with the experimental data in Figure 5a. Quantitative results can be better obtained by projecting the fit onto temporal (Figure 5c) and spectral (Figure 5d) domains. The solid red and blue fit curves in Figure 5c describe the dynamic trends in the pre-edge and $Fe^+$ ranges, respectively, very well. The residuals of the global fit are shown in Figure S6 in the SI. The temporal decomposition reveals that two exponential rise functions with characteristic time scales of $\tau_1$ < 25 fs (limited by the instrument response function) and $\tau_2$ = 240 ± 80 fs are adequate to fit the data. For the $Fe^+$ signal in Figure 5c, the two fit components are represented by the purple and yellow curves with no data points on them. Given that SFI can only occur during the pump pulse duration, we assign the 25 fs time scale to dynamics that occur during the initial ionization of the ferrocene molecule. The spectrum of this component as derived by the global fit is shown as the solid yellow line in the lower panel of Figure 5d. This spectrum essentially consists of one broad positive (absorption) feature, centered around 56 eV, and an extended negative (depletion) feature below ~52 eV. It is possible that there is an additional structure, in particular a bimodal distribution, but the signal-to-noise is insufficient to make any definitive statements. Since this component should mostly comprise signals from $FeCp_2^+$, we would expect it to match the long-time spectra found with very low NIR intensity, which is displayed for comparison as the dark red dashed curve in Figure 5d. Broadly speaking, this is the case: taking the peak as a whole, it matches up with the spectrum recorded at $2 \times 10^{13}$ W cm$^{-2}$. The intricacies of the peaks have been lost, presumably due to the impact of the large $Fe^+$ peak on the fitting routine, but there is broad agreement, particularly in the low energy edge of the peak. Similarities between the two spectra are consistent with the conclusion that the positive section of the rapidly emerging spectral component is primarily associated with the promptly created $FeCp_2^+$ ion, while the negative section indicates the depletion of the neutral parent molecule. The signal-to-noise levels are insufficient to distinguish between the dynamics of the $^2FeCp_2^+$ and $^4FeCp_2^+$ ions. In contrast, the spectrum of the more slowly rising component (purple curve in Figure 5d upper panel) is very reminiscent of the spectrum of $Fe^+$ atomic ions (dashed black curve),[39] but with an additional positive component in the pre-edge region. We therefore assign the majority of this component (beyond ~53 eV) to $Fe^+$ production following dissociation of the ferrocenium ion with simultaneous loss of



DOI: 10.1021/acs.jpca.6b09724
J. Phys. Chem. A 2016, 120, 9509−9518

both cyclopentadienyl rings. Within the quality of the data and the temporal resolution of the experiment (40 fs fwhm), we see no evidence of either a transient intermediate state[41−43] or of any spectral shifts that are sometimes associated with molecular dynamics.[20]

We have also considered the possibility that single ring loss may lead to products that are stable on a femtosecond time scale, but unstable on a time-of-flight time scale, that is, the possibility that the spectrum that we associate predominantly with $Fe^+$ may contain significant contributions from $FeCp^+$ that would dissociate on a time scale beyond the time range of our experiment but before detection in stationary ion yield measurements. This possibility has been addressed in two ways: first, we have calculated the Fe 3p absorption spectrum of the lowest energy single ring loss species, $^5FeCp^+$ (Figure 3e). Its spectrum is characterized by a broad feature at around 56 eV, which is inconsistent with the sharp double peak structure extending below 53 eV that we assign as $Fe^+$. In addition, the very low intensity of the $^5FeCp^+$ spectrum above ∼58 eV could most likely not compensate the parent molecule signal depletion as already noted in section 4.1 and discussed in more detail below. Second, an additional XUV difference spectrum has been recorded 250 ps after ionization (see Figure S5 in the SI). No significant changes compared to the 1 ps spectrum (green) at the same nominal pump intensity are apparent, suggesting that the majority of dynamics are complete in less than 1 ps, in accordance with the longest recovered time scale being $\tau_2$ = 240 fs.

## 5. DISCUSSION

**5.1. XUV Spectra of Ferrocenium Ions.** The XUV transient absorption spectra recorded at low pump pulse intensities (Figure 3d, red curve) should be composed almost entirely of XUV transitions in $FeCp_2^+$. To the best of our knowledge, the spectrum of this species at the iron $M_{2,3}$ edge has never been reported before. The main feature is rather broad, although it has some structure to it, exhibiting maxima at 53.0 and 55.7 eV. Comparing this spectrum to that of the atomic $Fe^+$ ion (Figure 3b, black curve) reveals that it is very similar in profile but shifted by 0.8 eV to lower energies. First-principles calculations find the double peak structure of $Fe^+$ can be loosely reproduced with a combination of the $4s^03d^7$ and $4s^13d^6$ configurations, while the $FeCp_2^+$ spectrum can be reproduced as a combination of $^2FeCp_2^+$ and $^4FeCp_2^+$ spin states.

From a molecular orbital point of view, it is perhaps not surprising that $FeCp_2^+$ and $Fe^+$ possess similar spectra. The frontier orbitals of ferrocene are nonbonding d orbitals predominantly associated with the metal center (Figure 4c),[13,16] so the hole density of ions created by SFI may be expected to mimic these orbitals. An $Fe^+$ ion possesses an almost half empty d shell ($4s^1$ $3d^6$ ground state configuration), so from the point of view of the iron, excitation to a nonbonding molecular d hole is likely rather similar to excitation to an atomic half-occupied d orbital. The chemical shift of 0.8 eV is likely the effect of the two aromatic cyclopentadienyl rings on the otherwise weakly perturbed 3d orbitals.

In contrast to other XUV transient absorption experiments,[5,20,42−45] an obvious ground state bleach feature associated with inner-shell transitions is not observable in the XUV spectra presented here. Intuitively, one may expect that ionization and dissociation of the molecule should result in a decrease of absorption with a spectral imprint similar to that of the ground state XUV absorption spectrum (Figure 3a), as is usually observed in these kinds of experiments. However, our calculations show that the 3p → LUMO transitions in $FeCp_2^+$ ions are rather similar to those of neutral $FeCp_2$ (Figure 3); hence, any prominent depletion features are most likely obscured by equally dominant product features. In fact, we see a minor signal enhancement in the parent spectral region, suggesting that the ions may in fact be stronger absorbers than the parent neutral in the 3p → valence region. Such a trend could perhaps be rationalized by an increased contribution of Fe 3d orbitals to the unoccupied molecular orbitals, relative to the contribution of the cyclopentadiene rings.[16] Note that some negative ΔOD sections are visible beyond 63 eV, which may be residual parent depletion.

**5.2. Dynamics and Dissociation Mechanism.** Two dynamic trends proceeding on two different time scales are observed in the transient XUV absorption experiments with ∼6 × $10^{13}$ W $cm^2$ pump intensity: instrument response limited creation of $FeCp_2^+$, and the appearance of $Fe^+$ ions within 240 fs. The latter time scale is significantly longer than the instrument response function of 40 fs, indicating that one or more dissociative state(s) are prepared and that complete dissociation does not occur during the presence of the strong NIR field. It is interesting to note that no delayed rise or stepwise kinetics are required to capture the $Fe^+$ transient. One might expect that the mechanism for $Fe^+$ appearance would involve first one cyclopentadienyl ring departing, to leave an unstable intermediate, followed by loss of the second ring.[19] If such a mechanism were active, an intermediate would probably be visible at early times and/or as a delayed onset of the $Fe^+$ signal. We note that the rapid rise of the $FeCp_2^+$ signal may mask some dynamics at very short delays, but we can most likely rule out any intermediates with lifetimes beyond the 40 fs instrument response function. This suggests that both rings depart from excited ferrocenium ions almost simultaneously. It is, in principle, possible that additional slow channels could lead to complete dissociation. We can, however, rule out any slow channels with time constants shorter than 250 ps (Figure S5).

The preference for double ring loss over single ring loss is likely a reflection of the electronic structure of $FeCp_2^+$. The bond energies of ferrocene and ferrocenium$^+$ have been determined using electron impact. In neutral $FeCp_2$, the loss of the first Cp ring requires 4 eV, and dissociation of the second requires a further 2.2 eV. On the other hand, in $FeCp_2^+$, the first ring is bound by 6.1 eV, but the second requires only an additional 1 eV to dissociate from the Fe atom.[46] At comparable laser intensities to this work, Yatsuhashi et al. found single ring loss to be around an order of magnitude less likely than double ring loss in the asymptotic limit of microsecond scale detection times.[19] The authors assumed that a sequential dissociation mechanism may account for the preference for double ring loss. The results presented here, however, suggest that the preference may instead be due to a very fast dissociation mechanism involving both rings, potentially because it is so easy to break the bond between the iron atom and the second ring. If both dissociation channels open at approximately equal energies, then we cannot make arguments based on numbers of photons absorbed in the SFI step, and instead, cross sections to available states will dominate the observed yields. It should be noted that absorption of eight photons is insufficient to cross the single ring loss threshold, while absorption of an additional photon provides sufficient


DOI: 10.1021/acs.jpca.6b09724
J. Phys. Chem. A 2016, 120, 9509−9518

energy for both single and double ring loss. Presumably, the single ring loss channel has a much smaller yield in the strong field conditions of the experiment presented here. As we observe no intermediates in the time-resolved spectrum, we cannot make any precise statements as to the character or nature of the dissociative electronic excited states.

In our experiments with ~$6 \times 10^{13}$ W cm$^{-2}$ NIR excitation, we have found evidence for only a single $Fe^+$ elimination channel which proceeds within 240 fs. As the complete dissociation occurs quicker than a rotational period (~2.6 ps at the temperatures of these experiments), and it is unlikely that the two Fe−Cp bonds are cleaved *exactly* simultaneously, this dissociation is best classified as a three-body asynchronous concerted decay.[47−49] There are two plausible mechanisms we can assign to this channel: (1) three-body Coulomb explosion of a highly charged precursor; or (2) rapid dissociation upon one or more dissociative electronic states, accessed either directly or via rapid state crossing (dissociative ionization). We can rule out a pure Coulomb explosion reaction simply from the dissociation lifetime. A simplistic classical Coulomb explosion model for $FeCp_2^{3+}$ dissociating into $Fe^+ + 2Cp^+$ indicates that, within 240 fs, the Fe−Cp bond length would have elongated over 10-fold. Therefore, a Coulomb explosion would produce a much shorter time constant than the 240 fs we observe. Additionally, any Coulomb explosion mechanism would require highly charged precursors, for which we see no evidence. Instead, we must conclude that the dissociation occurs via dissociative ionization from an excited state of the $FeCp_2^+$ monocation. The complexity of the strong field ionization process prevents us from making any concrete statement about the dissociative state(s), but there is no guarantee that it is a straightforward process, and curve crossing may be involved. Note that we also cannot conclusively determine whether the excited cation is prepared directly from the ground state, or if it is due to sequential excitation of $FeCp_2^+$ cations within the same laser pulse.

The pre-edge region ($h\nu$ < 53 eV) of the static XUV absorption spectrum of $FeCp_2$ has been assigned to the ionization of the valence states of ferrocene.[17,18] The early time depletion observed in this region can then be assigned to a depletion of the population of neutral $FeCp_2$ molecules. The recovery observed in this spectral region (Figure 5c, red line), however, suggests the emergence of fragments with valence ionization cross sections more comparable to the neutral parent molecule. The time scale of the recovery agrees very well with that of the $Fe^+$ production, and both are described by the same temporal evolution function $\mathbf{f}_n(t)$ in Figure 5. It thus appears that the partial recovery of the valence absorption signal may be associated with the emergence of fragments, following the cleavage of the C−Fe bond. A unique assignment of the identity of these fragments is not feasible with the available data. The recovery in this region may reflect contributions from valence ionization of $Fe^+$. The 3p pre-edge absorption of $Fe^+$ is ~15% as intense as its peak value at ~56.5 eV,[39] so a small contribution would be expected. Alternatively, one may speculate that since neutral hydrocarbon fragments should be produced concomitantly with $Fe^+$, it is possible that the pre-edge region gives some reflection of the production of these hydrocarbon fragments.

Finally, we can compare the effects of NIR SFI to photolysis using UV lasers. Using nanosecond lasers, fragmentation has been observed with wavelengths ranging from the visible to the deep UV.[50−54] A key distinction is that these experiments have sufficiently long laser pulses to ionize or further fragment any products of the initial dissociation. The general mechanism to give either single or double ring loss was found to be one of photon cycling, i.e., repeated absorption of a photon followed by internal conversion, until enough energy has been deposited to break a bond. Such a mechanism cannot apply in the case of a single femtosecond pulse,[55] but it is interesting to note that the presence of a photon cycling scheme implies that relaxation to the ground electronic state can occur on a few nanoseconds time scale. As we do not observe spectral changes out to 250 ps, we can conclude that, in the strong field case, such relaxation either does not occur, does not result in significant spectral changes, or takes significantly longer than 250 ps.

Previous femtosecond pump−probe experiments using UV wavelengths of 237−272 nm observed fragmentation of $FeCp_2$ within 200 fs.[56,57] In those experiments, fragments were created using a single photon pump and detected with a multiphoton probe. Both single and double ring loss were observed, in a roughly 1:2 ratio, respectively. On the basis of the similar dissociation lifetimes, it is tempting to draw a parallel between the UV and strong field excitation cases. However, in the UV experiments, $Fe^+$ ions were produced during the probe step from excitation of previously produced $FeCp_2^+$ cations, whereas in the XUV transient absorption experiments we cannot observe fragmentation induced by the probe pulse. Thus, despite the similar time scales, the process for $Fe^+$ production with UV and NIR strong field pulses is rather different, and a direct comparison is not possible.

## 6. CONCLUSIONS

Using femtosecond XUV transient absorption spectroscopy, the strong field ionization induced dissociation of ferrocene has been monitored from the point of view of the iron atom. At low field intensities (<$5 \times 10^{13}$ W cm$^{-2}$), $FeCp_2^+$ ions, in both doublet and quartet spin states, are by far the dominant observed species. The Fe 3p inner-shell absorption spectrum of ferrocenium ions is remarkably similar to that of singly charged iron ions, presumably due to the nonbonding nature of ferrocene frontier d orbitals. As the field strength is increased, the production of $Fe^+$ ions with a time constant of 240 fs is observed. This appearance time is significantly longer than the duration of the pump pulse, indicating that a dissociative state of the molecular cation is accessed. Intriguingly, both cyclopentadienyl rings depart from the iron center within this time with no evidence recorded for a single ring loss intermediate within the experimental response of 40 fs, indicating an asynchronous concerted decay process. We propose that the preference for double over single ring loss is due to the weak Fe−Cp bond strength of $FeCp^+$ (≈1 eV) compared to the total energy required to create $FeCp^+$ (≈13 eV), although SFI is insufficiently selective in the initial state preparation to probe this hypothesis in detail. We have also tested for the possibility that, at very long time delays, further fragmentation (possibly of a metastable $FeCp^+$ fragment) could occur. Spectra recorded at 1 and 250 ps exhibit no significant differences, indicating that the majority of dynamics are indeed complete on a hundreds of femtoseconds time scale.

The experiments add to a rich literature on ferrocene dissociation experiments, using SFI as the means of depositing energy. Previous studies nicely documented the final product distribution following SFI across a large span of NIR intensities.[19] With the use of XUV transient absorption techniques, we are now able to track the actual dissociation


DOI: 10.1021/acs.jpca.6b09724
J. Phys. Chem. A 2016, 120, 9509−9518

process, providing a complementary view of the strong field induced dynamics. The preference for double ring loss over single ring loss can be explained energetically, but further explorations into this prototypical organometallic system are required to fully understand its complex dissociation pathways.

## ■ ASSOCIATED CONTENT

### Supporting Information

The Supporting Information is available free of charge on the ACS Publications website at DOI: 10.1021/acs.jpca.6b09724.

Intensity dependent spectra with confidence intervals, detailed comparisons between TDDFT-TDA and DFT/ROCIS computed spectra, the computed spectrum of $^{2}FeCp_2^{+*}$, molecular orbital diagrams for $^{5}FeCp^{+}$, difference absorption spectra recorded at 250 ps, and residuals from the global fit (PDF)

## ■ AUTHOR INFORMATION


### Corresponding Author

*E-mail: ogessner@lbl.gov.

### ORCID

Adam S. Chatterley: 0000-0003-3847-5936

Stephen R. Leone: 0000-0003-4006-2292

### Present Addresses

A.S.C.: Dept. of Chemistry, Aarhus University, 8000 Aarhus C, Denmark.

F.L.: Institut für Experimentalphysik,Technische Universität Graz, 8010 Graz, Austria.


### Notes

The authors declare no competing financial interest.

## ■ ACKNOWLEDGMENTS

This work was supported by the U.S. Department of Energy, Office of Basic Energy Sciences, Chemical Sciences, Geosciences and Biosciences Division, through Contract No. DE-AC02-05CH11231. F.L. would like to acknowledge support by the Austrian Science Fund (FWF, Erwin Schrödinger Fellowship Grant No. J 3580-N20).

## ■ REFERENCES


(1) Kealy, T. J.; Pauson, P. L. A New Type of Organo-Iron Compound. *Nature* **1951**, *168*, 1039−1040.

(2) Werner, H. At Least 60 Years of Ferrocene: The Discovery and Rediscovery of the Sandwich Complexes. *Angew. Chem., Int. Ed.* **2012**, *51*, 6052−6058.

(3) Daeneke, T.; Kwon, T.-H.; Holmes, A. B.; Duffy, N. W.; Bach, U.; Spiccia, L. High-Efficiency Dye-Sensitized Solar Vells with Ferrocene-Based Electrolytes. *Nat. Chem.* **2011**, *3*, 213−217.

(4) Loh, Z.-H.; Leone, S. R. Capturing Ultrafast Quantum Dynamics with Femtosecond and Attosecond X-ray Core-Level Absorption Spectroscopy. *J. Phys. Chem. Lett.* **2013**, *4*, 292−302.

(5) Lin, M.-F.; Pfeiffer, A. N.; Neumark, D. M.; Leone, S. R.; Gessner, O. Strong-Field Induced XUV Transmission and Multiplet Splitting in 4d−16p Core-Excited Xe Studied by Femtosecond XUV Transient Absorption Spectroscopy. *J. Chem. Phys.* **2012**, *137*, 244305.

(6) Ivanov, M. Y.; Spanner, M.; Smirnova, O. Anatomy of Strong Field Ionization. *J. Mod. Opt.* **2005**, *52*, 165−184.

(7) Corkum, P. B. Plasma Perspective on Strong Field Multiphoton Ionization. *Phys. Rev. Lett.* **1993**, *71*, 1994−1997.

(8) Armstrong, A. T.; Smith, F.; Elder, E.; McGlynn, S. P. Electronic Absorption Spectrum of Ferrocene. *J. Chem. Phys.* **1967**, *46*, 4321−4328.

(9) Blackburn, F. R.; Snavely, D. L.; Oref, I. Visible Absorption Spectrum of Gaseous Ferrocene. *Chem. Phys. Lett.* **1991**, *178*, 538−542.

(10) Ketkov, S. Y.; Domrachev, G. A. Ultraviolet Vapor-Phase Absorption-Spectra of d6-Metallocenes. *J. Organomet. Chem.* **1991**, *420*, 67−77.

(11) Scuppa, S.; Orian, L.; Dini, D.; Santi, S.; Meneghetti, M. Nonlinear Absorption Properties and Excited State Dynamics of Ferrocene. *J. Phys. Chem. A* **2009**, *113*, 9286−9294.

(12) Zerner, M. C.; Loew, G. H.; Kirchner, R. F.; Mueller-Westerhoff, U. T. An Intermediate Neglect of Differential Overlap Technique for Spectroscopy of Transition-metal Complexes. Ferrocene. *J. Am. Chem. Soc.* **1980**, *102*, 589−599.

(13) Derat, E.; Costuas, K.; Volatron, F. Theory of Ferrocenyl Compounds. In *PATAI'S Chemistry of Functional Groups*; John Wiley & Sons, Ltd.: 2009.

(14) Cattenacci, G.; Aschi, M.; Graziano, G.; Amadei, A. A Theoretical Study on the Spectral and Electrochemical Properties of Ferrocene in Different Solvents. *Inorg. Chim. Acta* **2013**, *407*, 82−90.

(15) Salzner, U. Quantitatively Correct UV-vis Spectrum of Ferrocene with TDB3LYP. *J. Chem. Theory Comput.* **2013**, *9*, 4064−4073.

(16) Lancaster, K. M.; Finkelstein, K. D.; DeBeer, S. K$\beta$ X-ray Emission Spectroscopy Offers Unique Chemical Bonding Insights: Revisiting the Electronic Structure of Ferrocene. *Inorg. Chem.* **2011**, *50*, 6767−6774.

(17) Wen, A. T.; Ruehl, E.; Hitchcock, A. P. Inner-Shell Excitation of Organoiron Compounds by Electron Impact. *Organometallics* **1992**, *11*, 2559−2569.

(18) Tamenori, Y.; Boo, B. H.; Koyano, I. Dissociative Photoionization of Ferrocene in the Fe:3p Inner-Valence Region. *J. Electron Spectrosc. Relat. Phenom.* **1999**, *101−103*, 87−91.

(19) Yatsuhashi, T.; Murakami, E.; Nakashima, N. $Fe^{z+}$ (z = 1−6) Generation from Ferrocene. *Phys. Chem. Chem. Phys.* **2011**, *13*, 4234−4238.

(20) Lin, M.-F.; Neumark, D. M.; Gessner, O.; Leone, S. R. Ionization and Dissociation Dynamics of Vinyl Bromide Probed by Femtosecond Extreme Ultraviolet Transient Absorption Spectroscopy. *J. Chem. Phys.* **2014**, *140*, 064311.

(21) Hankin, S. M.; Villeneuve, D. M.; Corkum, P. B.; Rayner, D. M. Intense-Field Laser Ionization Rates in Atoms and Molecules. *Phys. Rev. A: At., Mol., Opt. Phys.* **2001**, *64*, 013405.

(22) Macklin, J. J.; Kmetec, J. D.; Gordon, C. L. High-Order Harmonic Generation Using Intense Femtosecond Pulses. *Phys. Rev. Lett.* **1993**, *70*, 766−769.

(23) Runge, E.; Gross, E. K. U. Density-Functional Theory for Time-Dependent Systems. *Phys. Rev. Lett.* **1984**, *52*, 997−1000.

(24) Hohenberg, P.; Kohn, W. Inhomogeneous Electron Gas. *Phys. Rev.* **1964**, *136*, B864−B871.

(25) Kohn, W.; Sham, L. J. Self-Consistent Equations Including Exchange and Correlation Effects. *Phys. Rev.* **1965**, *140*, A1133−A1138.

(26) Neese, F. The ORCA Program System. *Wiley Interdisciplinary Reviews: Computational Molecular Science* **2012**, *2*, 73−78.

(27) Lee, C.; Yang, W.; Parr, R. G. Development of the Colle-Salvetti Correlation-energy Formula into a Functional of the Electron Density. *Phys. Rev. B: Condens. Matter Mater. Phys.* **1988**, *37*, 785−789.

(28) Becke, A. D. Density-Functional Thermochemistry. III. The Role of Exact Exchange. *J. Chem. Phys.* **1993**, *98*, 5648−5652.

(29) Weigend, F.; Ahlrichs, R. Balanced Basis Sets of Split Valence, Triple Zeta Valence and Quadruple Zeta Valence Quality for H to Rn: Design and Assessment of Accuracy. *Phys. Chem. Chem. Phys.* **2005**, *7*, 3297−3305.

(30) Vahtras, O.; Almlöf, J.; Feyereisen, M. W. Integral Approximations for LCAO-SCF Calculations. *Chem. Phys. Lett.* **1993**, *213*, 514−518.

(31) Eichkorn, K.; Treutler, O.; Öhm, H.; Häser, M.; Ahlrichs, R. Auxiliary Basis Sets to Approximate Coulomb Potentials. *Chem. Phys. Lett.* **1995**, *240*, 283−290.




DOI: 10.1021/acs.jpca.6b09724
J. Phys. Chem. A 2016, 120, 9509−9518

(32) Weigend, F. Accurate Coulomb-Fitting Basis sets for H to Rn. *Phys. Chem. Chem. Phys.* **2006**, *8*, 1057−1065.
(33) Zhang, Y.; Biggs, J. D.; Healion, D.; Govind, N.; Mukamel, S. Core and Valence Excitations in Resonant X-Ray Spectroscopy Using Restricted Excitation Window Time-Dependent Density Functional Theory. *J. Chem. Phys.* **2012**, *137*, 194306.
(34) Casida, M. E. In *Recent Advances in Density Functional Methods*; Chong, D. P., Ed.; World Scientific: Singapore, 1995; pp 155−192.
(35) Shao, Y.; Gan, Z.; Epifanovsky, E.; Gilbert, A. T. B.; Wormit, M.; Kussmann, J.; Lange, A. W.; Behn, A.; Deng, J.; Feng, X.; et al. Advances in Molecular Quantum Chemistry Contained in the Q-Chem 4 Program Package. *Mol. Phys.* **2015**, *113*, 184−215.
(36) Hirata, S.; Head-Gordon, M. Time-Dependent Density Functional Theory Within the Tamm−Dancoff Approximation. *Chem. Phys. Lett.* **1999**, *314*, 291−299.
(37) Huang, D.-J.; Riffe, D. M.; Erskine, J. L. Simultaneous Determination of Fe 3p Spin-Orbit and Exchange Splittings in Photoemission. *Phys. Rev. B: Condens. Matter Mater. Phys.* **1995**, *51*, 15170−15179.
(38) Roemelt, M.; Maganas, D.; DeBeer, S.; Neese, F. A Combined DFT and Restricted Open-Shell Configuration Interaction Method Including Spin-Orbit Coupling: Application to Transition Metal L-edge X-Ray Absorption Spectroscopy. *J. Chem. Phys.* **2013**, *138*, 204101.
(39) Kjeldsen, H.; Kristensen, B.; Folkmann, F.; Andersen, T. Measurements of the Absolute Photoionization Cross Section of Fe + Ions from 15.8 to 180 eV. *J. Phys. B: At., Mol. Opt. Phys.* **2002**, *35*, 3655.
(40) El Hassan, N.; Bizau, J. M.; Blancard, C.; Cossé, P.; Cubaynes, D.; Faussurier, G.; Folkmann, F. Photoionization Cross Sections of Iron Isonuclear Sequence ions: $Fe^{2+}$ to $Fe^{3+}$. *Phys. Rev. A: At., Mol., Opt. Phys.* **2009**, *79*, 033415.
(41) Attar, A. R.; Bhattacherjee, A.; Leone, S. R. Direct Observation of the Transition-State Region in the Photodissociation of CH3I by Femtosecond Extreme Ultraviolet Transient Absorption Spectroscopy. *J. Phys. Chem. Lett.* **2015**, *6*, 5072−5077.
(42) Lackner, F.; Chatterley, A. S.; Pemmaraju, C. D.; Closser, K. D.; Prendergast, D.; Neumark, D. M.; Leone, S. R.; Gessner, O. Direct Observation of Ring-Opening Dynamics in Strong-Field Ionized Selenophene Using Femtosecond Inner-Shell Absorption Spectroscopy. *J. Chem. Phys.* 2016, submitted.
(43) Chatterley, A. S.; Lackner, F.; Neumark, D. M.; Leone, S. R.; Gessner, O. Tracking Dissociation Dynamics of Strong-Field Ionized 1,2-dibromoethane with Femtosecond XUV Transient Absorption Spectroscopy. *Phys. Chem. Chem. Phys.* **2016**, *18*, 14644−14653.
(44) Attar, A. R.; Piticco, L.; Leone, S. R. Core-to-Valence Spectroscopic Detection of the $CH_2Br$ Radical and Element-Specific Femtosecond Photodissociation Dynamics of $CH_2IBr$. *J. Chem. Phys.* **2014**, *141*, 164308.
(45) Loh, Z.-H.; Leone, S. R. Ultrafast Strong-field Dissociative Ionization Dynamics of $CH_2Br_2$ Probed by Femtosecond Soft X-Ray Transient Absorption Spectroscopy. *J. Chem. Phys.* **2008**, *128*, 204302.
(46) Barfuss, S.; Grade, M.; Hirschwald, W.; Rosinger, W.; Boag, N. M.; Driscoll, D. C.; Dowben, P. A. The Stability and Decomposition of Gaseous Chloroferrocenes. *J. Vac. Sci. Technol., A* **1987**, *5*, 1451−1455.
(47) Strauss, C. E. M.; Houston, P. L. Correlations Without Coincidence Measurements: Deciding Between Stepwise and Concerted Dissociation Mechanisms for ABC.-+. A + B + C. *J. Phys. Chem.* **1990**, *94*, 8751−8762.
(48) Maul, C.; Gericke, K.-H. Photo Induced Three Body Decay. *Int. Rev. Phys. Chem.* **1997**, *16*, 1−79.
(49) Maul, C.; Gericke, K.-H. Aspects of Photoinduced Molecular Three-Body Decay. *J. Phys. Chem. A* **2000**, *104*, 2531−2541.
(50) Ketkov, S. Y.; Selzle, H. l.; Schlag, E. W. Nanosecond Multiphoton Ionization Spectroscopy of Transition-Metal Sandwich Compounds: a Comparative Study of Nickelocene, Ferrocene and bis(η6-benzene)chromium. *Mol. Phys.* **2004**, *102*, 1749−1757.
(51) Ketkov, S. Y.; Selzle, H. L.; Schlag, E. W.; Domrachev, G. A. Mass-Resolved Nanosecond Laser Spectroscopy of Jet-Cooled Ferrocene in the Region of the 3dz2 → R4px,y One-Photon Rydberg Transition. *J. Phys. Chem. A* **2003**, *107*, 4041−4045.
(52) Opitz, J.; Bruch, D.; von Bünau, G. Multiphoton Excitation of Ferrocene and Vanadocene at 351 nm in Comparison with 248 and 193 nm. Wavelength Dependent Competition Between Ionization and Dissociation. *Org. Mass Spectrom.* **1993**, *28*, 405−411.
(53) Opitz, J.; Harter, P. Multiphoton Ionization of Vanadocene and Ferrocene at 248 and 193 nm Wavelength-Dependent Competition Between Dissociation and Ionization. *Int. J. Mass Spectrom. Ion Processes* **1992**, *121*, 183−199.
(54) Ray, U.; Hou, H. Q.; Zhang, Z.; Schwarz, W.; Vernon, M. A Crossed Laser-molecular Beam Study of the One and Two Photon Dissociation Dynamics of Ferrocene at 193 and 248 nm. *J. Chem. Phys.* **1989**, *90*, 4248−4257.
(55) Grun, C.; Weikhardt, C.; Grotemeyer, J. Letter: Multiphoton Ionisation Mass Spectrometry of Metal Organic Compounds: Avoiding the Ultrafast Neutral Dissociation Channels by Femtosecond Laser Activation. *Eur. Mass Spectrom.* **1996**, *2*, 197−202.
(56) Clara, M.; Braun, J. E.; Hellerer, T.; Neusser, H. J. Femtosecond Laser Mass Spectroscopy of Ferrocenes: Photochemical Stabilization by Bridged Cyclopentadienyl Rings? *Int. J. Mass Spectrom.* **2000**, *203*, 71−81.
(57) Clara, M.; Neusser, H. J. Ultrafast Dissociation Dynamics of Ferrocene and [3]-Ferrocenophan. *J. Phys. Chem. A* **2001**, *105*, 5577−5585.


DOI: 10.1021/acs.jpca.6b09724
*J. Phys. Chem. A* 2016, 120, 9509−9518